Brain Topography (2021) 34:664–680
https://doi.org/10.1007/s10548-021-00860-2

ORIGINAL PAPER

Free-Field Cortical Steady-State Evoked Potentials in Cochlear Implant Users

Razieh Alemi[1,2,3] · **Sylvie Nozaradan**[4] · **Alexandre Lehmann**[1,2,3]

Received: 4 January 2021 / Accepted: 18 June 2021 / Published online: 29 June 2021

Abstract

Auditory steady-state evoked potentials (SS-EPs) are phase-locked neural responses to periodic stimuli, believed to reflect specific neural generators. As an objective measure, steady-state responses have been used in different clinical settings, including measuring hearing thresholds of normal and hearing-impaired subjects. Recent studies are in favor of recording these responses as a part of the cochlear implant (CI) device-fitting procedure. Considering these potential benefits, the goals of the present study were to assess the feasibility of recording free-field SS-EPs in CI users and to compare their characteristics between CI users and controls. By taking advantage of a recently developed dual-frequency tagging method, we attempted to record subcortical and cortical SS-EPs from adult CI users and controls and measured reliable subcortical and cortical SS-EPs in the control group. Independent component analysis (ICA) was used to remove CI stimulation artifacts, yet subcortical responses of several CIs were heavily contaminated by these artifacts. Consequently, only cortical SS-EPs were compared between groups, which were found to be larger in the controls. The lower cortical SS-EPs' amplitude in CI users might indicate a reduction in neural synchrony evoked by the modulation rate of the auditory input across different neural assemblies in the auditory pathway. The brain topographies of cortical auditory SS-EPs, the time course of cortical responses, and the reconstructed cortical maps were highly similar between groups, confirming their neural origin and possibility to obtain such responses also in CI recipients. As for subcortical SS-EPs, our results highlight a need for sophisticated denoising algorithms to pinpoint and remove artifactual components from the biological response.

Keywords Cochlear implant · Auditory steady-state evoked potentials · Auditory hierarchy · Frequency-tagging approach

Abbreviations

CIs	Cochlear Implants
EEG	Electroencephalography
ASSR	Auditory Steady-State Responses
EASSR	Electrically Evoked ASSR
SS-Eps	Steady-State Evoked Potentials
ICA	Independent Component Analysis
DFT	Discrete Fourier transform
FFT	Fast Fourier transform

Introduction

In normal-hearing individuals, incoming sounds are processed through the different stages of the auditory processing hierarchy, from mechanical conduction to cortical processing. In individuals with severe sensorineural hearing loss, cochlear implants (CIs) bypass the dysfunctional cochlea by directly stimulating the auditory nerve via amplitude-modulated pulse trains delivered through an intracochlear electrode array (Clark 2004). Despite significant improvement in the quality of oral communication of CI recipients (Hirschfelder et al. 2008), substantial individual differences remain with regards to auditory processing outcomes (Glennon et al. 2020).

Handling Editor: Claude Alain.

✉ Razieh Alemi
razieh.alemi@mail.mcgill.ca;
razieh.alemi@mail.concordia.ca

1 Faculty of Medicine, Department of Otolaryngology, McGill University, Montreal, QC, Canada

2 Centre for Research On Brain, Language & Music (CRBLM), Montreal, Canada

3 International Laboratory for Brain, Music & Sound Research (BRAMS), Montreal, QC, Canada

4 Institute of Neuroscience (IONS), Université Catholique de Louvain (UCL), Ottignies-Louvain-la-Neuve, Belgium

Objective measures can provide deep insight into specific hierarchical stages of auditory neural processing (Picton et al. 1974), and thus could be used to investigate neural sites that potentially underlie the large variability in CI outcomes. Steady-state responses (often called auditory steady-state responses or ASSRs) recorded with electroencephalography (EEG) from the head surface are particularly interesting objective measures of auditory function because they represent phase-locked neural responses to periodic continuous stimuli.

Depending on the stimulus feature that is periodically modulated, these steady-state responses are believed to reflect activity from specific neural generators (Picton et al. 2003; Zoefel et al. 2018). With respect to amplitude modulation and the frequency range of this modulation, cortical areas are more prone to entrain to low-frequency modulations (< 20 Hz) (Liégeois-Chauvel et al. 2004). Subcortical regions are more sensitive to high-frequency modulations (> 80 Hz) (Bidelman 2015; Coffey et al. 2019), and mid-range modulation frequencies between 30 and 60 Hz can lead to nonspecific and mixed responses from all parts of the auditory hierarchy (Purcell et al. 2004). Therefore, the modulation frequency of the stimulus can be used to probe the source of electrophysiological activity within the auditory processing hierarchy (Picton et al. 1974, 2003; Herdman et al. 2002) and could be regarded as an indicator to determine the source of electrophysiological evoked-responses (Herdman et al. 2002; Picton et al. 2003; Luke et al. 2017).

Steady-state responses have been used to evaluate temporal envelope coding of auditory stimuli (Rees et al. 1986), multiple hearing frequencies (Picton et al. 2003), and speech processing (Liégeois-Chauvel et al. 2004) in normal-hearing individuals. In addition, these responses have been used to examine hearing thresholds of adolescent CI users (Torres-Fortuny et al. 2018) and the hearing-impaired population, as a part of an evaluation procedure for CI candidacy (Kuwada et al. 1986; Milford & Birchall 1989; Rance et al. 1993, 1998; Rance & Briggs 2002; Luts et al. 2006; Van Maanen & Stapells 2010). A recent paper recommended considering these responses as a tool to predict clinical outcomes of a CI surgery (Gransier et al. 2020). Moreover, numerous studies have suggested the potential benefit of measuring steady-state responses during CI device fitting procedures (Hofmann & Wouters 2010; Deprez et al. 2014; Gransier et al. 2016; Van Eeckhoutte et al. 2018).

Hofmann and Wouters (2010) measured electrically evoked (E) ASSRs to low-rate pulse trains from CI users and observed that the amplitudes of the elicited responses in CI users were similar to ASSRs recorded from normal hearing participants. In a follow-up study using high-rate amplitude and phase-width modulated pulse trains, the authors showed a strong correlation between EASSRs and hearing threshold levels (Hofmann & Wouters 2012). Similarly, Gransier et al. 2016 used a wide range of amplitude-modulated frequency stimuli (1–100 Hz) to measure EASSRs from six CI users. The authors reported that the highest amplitudes were recorded in response to 30–50 Hz modulation frequencies, whereas electrical stimulation within the 80–100 Hz range led to limited responses.

Both the generalization of the above-mentioned findings to everyday functional outcomes of patients and their translation to a large scale as a clinical tool may be somewhat limited because auditory stimuli were presented using direct sound streaming to the CI electrode array in all experiments. Neural responses elicited through bypassing the sound processor of the CI device might not reflect the naturalistic daily experience of CI users. In contrast, free-field stimulation is more realistic as it includes background noise, compression, and other processing into the final electrical stimulus. In addition, the direct streaming of the auditory signal to the speech processor is not widely available across the different models and brands worn by patients.

In this context, we addressed three questions in the current study. First, whether it is possible to record auditory steady-state evoked potentials (SS-EPs) from CI users while presenting the auditory stimuli from a loudspeaker (i.e., free-field stimulation). To answer this question, we took advantage of a recently developed frequency-tagging EEG method, a method that can be seen as an extension of previous ASSR designs. This approach allows us to carefully examine the dynamic nature of sound processing at different stages of the auditory hierarchy (Nozaradan 2014). The frequency-tagging EEG method follows the logic that presenting a stimulus with a fixed-rate repetition leads to a response with a periodic time course directly related to the stimulation frequency (Adrian & Matthews, 1934). This being said, the brain does not generate a response merely mirroring the stimulus, i.e., a linear reflection of stimulus frequency, but rather shows some nonlinear neural processing (Norcia et al. 2015; Tal et al. 2017; Nozaradan et al. 2017, 2018; Zoefel et al. 2018). The frequency-tagging approach provides a relatively direct way of investigating these processes by mapping the frequency content of the input with the neural output frequency content (Norcia et al. 2015; Nozaradan et al., 2018; Rossion et al. 2020).

The frequency-tagging technique possesses many advantages that make it potentially better than simple analysis techniques, including the possibility of presenting various frequency rates or multiple stimuli with a direct quantification of the evoked responses. These processing capacities led the researchers to benefit from this technique to examine both low- and high-level neural sensory processing relevant to visual (Regan, 1966; Müller et al., 2006; Rossion & Boremanse, 2011; Beck et al. 2018; Zhigalov et al. 2019) or auditory (Nozaradan et al. 2011, 2014, 2016, 2018; Lenc et al., 2020) modalities. These advantages from the

frequency-tagging approach provided us with an opportunity to expand the first question of our study and inquire as to whether the topographical distribution of the SS-EPs elicited by the modulation of high and low frequencies are similar across CI users and their matched controls. To this aim, we used a recent adaptation of the frequency-tagging approach, namely a dual frequency-tagging method as an attempt to include multiple amplitude modulations presented concomitantly in order to "tag" cortical and subcortical auditory responses at the same time (Lehmann et al. 2016; Nozaradan et al. 2016a, b, 2018; Lenc et al., 2020). Therefore, the third question we addressed here was whether the amplitude of SS-EPs recorded from CI users is different from those obtained from their matched controls at both hierarchical levels.

A challenge when recording EEG in this population is the fact the CIs induce large electrical artifacts that contaminate the signal. Reliable detection of neural responses from CI users' EEG remains an issue because physiological responses and CI stimulation artifacts are time-locked together (Gilley et al., 2006). This becomes even more problematic when dealing with long-duration stimuli and steady-state responses. The blanking technique (Hofmann & Wouters, 2010, 2012; Gransier et al., 2016; Deprez et al., 2017a) and independent component analysis (ICA) (Deprez et al., 2014, 2017b; Attina et al., 2017; Mina et al., 2017) have been the two most used artifact removal approaches, aiming to disentangle true neural responses from CI stimulation artifacts in ASSR designs. The blanking technique uses linear interpolation between pre- and post-stimulus samples to remove CI-stimulation artifacts, whereas ICA assumes that artifacts and evoked responses have independent spatial localizations that could be disentangled from each other (Makeig et al. 1996). In the current study, the ICA technique was used as the blanking technique cannot be used with free-field stimulus presentation. In order to use the blanking method, the CI-induced artifacts should be shorter than the inter-pulse interval (Deprez et al. 2016), a stimulation parameter that cannot be controlled when using free-field presentation.

Method and Materials

Participants

Fifteen CI users (8 females, mean age: 41.87 ± 13.17) and fifteen age and sex-matched controls (8 females, mean age: 41.93 ± 13.82) participated in this study (Table 1). The mean age of participants at the time of CI surgery was 33.13 ± 16.23 years. CI users had a history of 10.93 ± 10.15 years of hearing loss duration before CI surgery, and 8.93 ± 6.35 years of CI experience. Among the participants in the CI group, two participants had bilateral CIs, eight participants had their implant on the right side, and five participants had a left-side CI device. CI users received their implants as candidates with severe to profound bilateral hearing loss, none of them had residual hearing in the implanted ear. The two bilateral CI users had both their implants active at the time of testing. All other participants had only one CI and did not wear a hearing aid on the other side, so that the non-CI ear was profoundly deaf.

Table 1 Demographic data of CI users

Code	Age (Yrs)	Hearing loss duration (Yrs)	CI experience (Yrs)	Device	Speech Recognition score (%)
CI01	43	37	7	Cochlear	34
CI02	19	12	10	Advanced Bionics	72
CI03	23	23	21	Cochlear	33
CI04	35	11	9	MED-EL	33
CI05	56	3	3	MED-EL	44
CI06	33	33	17	Advanced Bionics	52
CI07*	53	20	7	Advanced Bionics	68
CI08*	43	13	5	Advanced Bionics	34
CI09	47	14	9	Cochlear	56
CI10	51	44	17	Advanced Bionics	56
CI11	41	20	17	Advanced Bionics	58
CI12	20	19	1	Advanced Bionics	36
CI13	58	10	3	Cochlear	90
CI14	54	12	7	Cochlear	14
CI15	52	27	1	Cochlear	80

*Bilateral CI user

Speech recognition scores of CI users were assessed using a validated list of fifty phonetically balanced French words (Picard, 1997). This test was selected based on its availability in International French and its ease of administration. Only CI users underwent this test because we anticipated a ceiling effect in the control group. The behavioral test was performed in a sound-attenuating room in a separate test session from the EEG recording. To measure this score, an open-set of pre-recorded monosyllable words was presented to CI users in free-field at 70 dB SPL with a fixed presentation rate. Participants were asked to repeat, after each word, what they heard as accurately as possible. The scores were calculated based on the percent of correctly repeated words. All controls had no history of hearing disorder and had a normal or corrected-to-normal vision. Participants with a self-reported neurological, motor, or psychological disorders were excluded from the study. All participants gave written informed consent and received compensation for their participation. The Research Ethics Board of the Centre for Research in Rehabilitation of Greater Montreal approved this study (CRIR-985–0714). CI users were recruited through the Raymond-Dewar Institute and the MAB-MacKay Rehabilitation Center in Montreal.

Stimulus and Parameters

Sixteen repetitions of 30-s isochronous sequences of complex tones were used as the auditory stimuli. A silent interstimulus interval of six seconds separated the sequences. Each stimulus consisted of a 165 Hz fundamental frequency auditory tone along with its four primary harmonics and was amplitude modulated by a percussive-like Hanning window with a 2.4 Hz periodicity, consisting of exactly 72 periods, using an asymmetrical Hanning envelope (12 ms rise time and 404 ms fall time with a modulation depth of 75 percent, as in Nozaradan et al. (2016a, b)) (Fig. 1). Furthermore, recent studies showed that measurable SS-EPs are reliably elicited at this frequency (Henry & Obleser 2012; Nozaradan et al. 2011, 2015, 2016). In addition, the 165 Hz carrier tone was selected because it is believed that SS-EP responses at

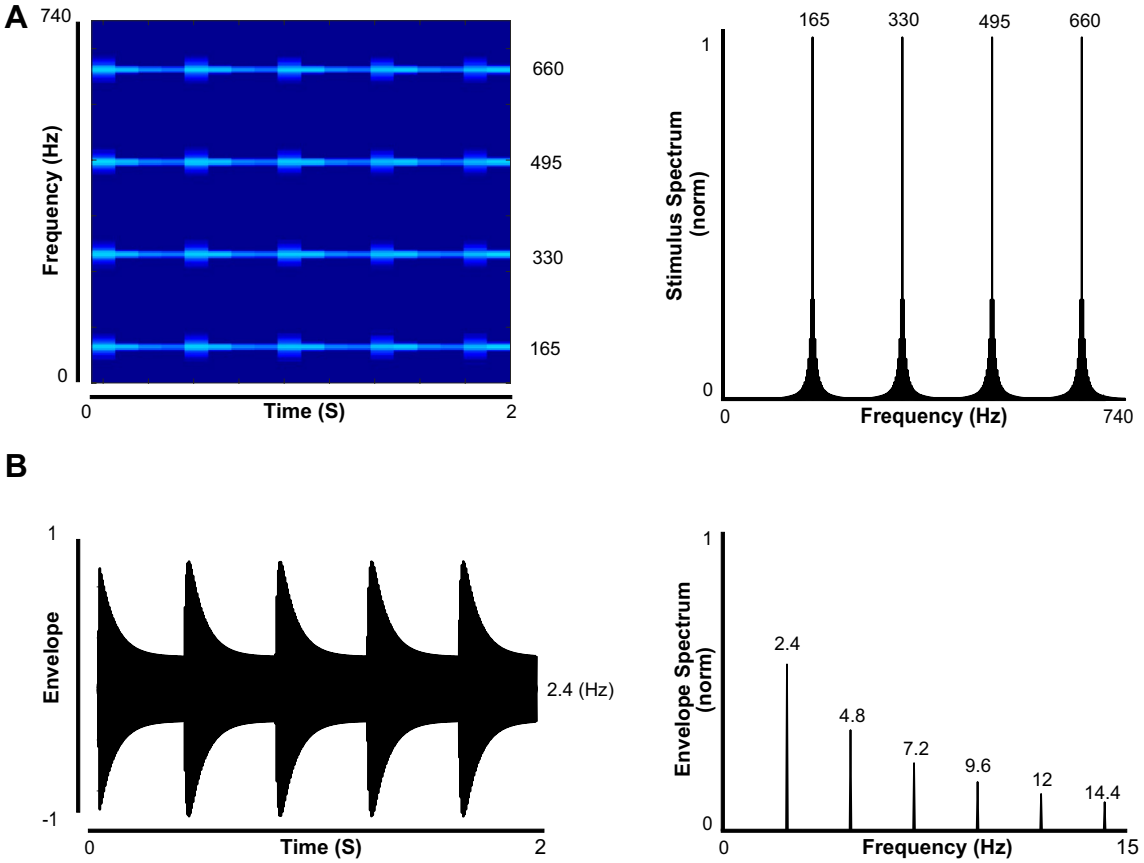

Fig. 1 Experimental design and stimulus: The complex tone (165 Hz fundamental frequency and its four harmonics) was amplitude-modulated at 2.4 Hz. A. Time–frequency extraction and the spectrum of the stimulus. The spectrum of the sound stimulus (right panel) exhibits its four peaks at the fundamental frequency and its harmonics, each flanked by sidebands at ± 2.4 Hz and harmonics. B. Excerpt of the envelope (with the periodic non-sinusoidal amplitude modulation) and frequency spectrum (right panel) with peaks at 2.4 Hz and its harmonics

this modulation frequency mostly originate from the subcortical areas (Skoe & Kraus 2010a). Prior studies showed that the higher auditory processing centers have limited capacity to track the high-frequency modulations, whereas lower processing centers, and more specifically, inferior colliculus, are the main generators in neural entrainment to high-frequency modulations (Coffey et al. 2019).

The auditory stimuli were generated and delivered to the participants using a programmable signal processor (RX6, Tucker Davis Technology, USA) controlled by custom scripts in MATLAB (The MathWorks, Natick, MA, USA). This apparatus enables sub-millisecond accurate synchronization between EEG recording and stimulus presentation. To prevent potential electrical artifacts at the frequency of the sound stimulus, the auditory stimuli were presented using inverted polarity on every other trial (Picton & John 2004; Hofmann & Wouters 2010; Skoe & Kraus 2010b). Stimuli were presented at 70 dB SPL from a single loudspeaker positioned at ear level, 1.2 m away from participants. Sound calibration was done using a SoundPro sound level meter (model DL 1/3 Octave Datalogging RTA, Quest, Bensenville, Illinois, USA) and was performed using a fast rate mode with an A-weighting frequency filter in an identical manner to our earlier work (Alemi & Lehmann 2019). The location of the loudspeaker was adjusted based on the implanted side of the CI users; consequently, the proportion of right/left side presentations for control participants was matched. In the CI group, the speech processor of participants was kept on the "on position," and the magnet was kept in place. All the participants in the control group had bilateral hearing with no masking.

EEG Recording

Participants were seated in a comfortable chair in a sound-attenuating and electromagnetically shielded room. To reduce muscle artifacts, participants were asked to remain awake and immobile. The EEG was recorded from 64 active Ag–AgCl electrodes placed over the scalp according to the international 10–10 electrode placement system (ActiveTwo, Biosemi, The Netherlands). Two bipolar electrodes were placed on the lateral canthi and on the superior and inferior orbits to record horizontal and vertical eye movements. Two other electrodes were placed on the right and left mastoids as the reference electrodes (Michel et al. 2004; Yao 2001). In CI participants, to avoid damaging the antenna with gel, the electrodes closest to it were not connected (between 1 and 3 electrodes, generally similar across participants for the left or right sides).

The impedance transformation on the electrode was provided by the ActiveTwo system, which allowed us to have low-noise recordings free of interference currents. Reference-free electrode signals were amplified using an ActiveTwo amplifier (BioSemi) and sampled at 8,192 Hz. The average potential was kept close to the voltage of the analog to digital converter reference in the AD-box (www.biosemi.com). The signal was recorded and stored for offline analysis using the BioSemi ActiView software.

Data Analysis

Preprocessing

Continuous EEG recordings were preprocessed using the EEGLAB toolbox (Delorme & Makeig 2004) running under MATLAB 2017b (The MathWorks, Natick, MA, USA). First, the signal was referenced offline to the average mastoids, a standard montage to measure brainstem and cortical auditory responses (Murray et al. 2008; Skoe & Kraus 2010b), and then resampled at 2,048 Hz for further processing. All channels were then filtered using a 0.1 Hz high-pass IIR Butterworth zero-phase filter (24 dB/octave, 4th order) to remove slow drifts in the recordings. EEG signals were visually inspected by the first author. On average, 3.4 ($\pm$2.1) channels in the CI group, which were either disconnected due to the CI device or marked as noisy channels, and 1.8 ($\pm$1.3) channels in controls, marked as flat or noisy channels, were initially discarded to be later interpolated. Prior to segmenting, EEG events were shifted in time to account for the sound air travel and digital to analog converter delay (1.92 ms). Continuous EEG was segmented into epochs from -2 s to + 30 s relative to the onset of the auditory stimulus. A baseline correction was applied by subtracting the averaged amplitude measured from -1.6 to -0.2 s relative to the onset of the auditory stimulus to the amplitude of each epoch. Finally, sixteen segments were extracted based on a 0 to + 30 s window (with zero being the onset of the stimulus). Eye blinks and muscular movements were corrected using the ICA algorithm ("runica" function of the Infomax algorithm implemented in EEGLAB) (Makeig & Onton 2011). On average, 3 ($\pm$0.9) and 3 ($\pm$1.6) ICA components were discarded specifically due to eye-related artifacts in the CI group and controls, respectively.

CI-Induced Artifact Removal

There are two methods to identify and remove the artifactual components from the biological signals: automatic and manual identification (Viola et al., 2012; Tamburro et al. 2021). The automatic approach relies on some pre-defined categorizations for pinpointing the artifactual components. However, there is still debate on the general application of these techniques because none of them considers a complete number of IC features to combine all the physiological artifacts (Echtioui et al. 2020).

One potential challenge in recording EEG in CI users is dealing with device-related electrical artifacts (Li et al. 2010). It has been argued that the artifacts are caused by both the radio frequency communication link and the electrical stimulation pulses produced by CI devices. These artifacts might change response properties, i.e., shape or amplitude, and obscure the expected biological response (Martin 2007), especially in response to complex and high-rate auditory stimuli (Jeng et al. 2007; Li et al. 2010). One strategy to remove these artifacts is to use one of the several methods already being used to separate biological artifacts from the neural responses recorded via multichannel EEG systems. At present, ICA algorithms are one of the most efficient denoising methods to eliminate electrical stimulation artifacts from the neural responses in different multichannel EEG paradigms such as transient cortical potentials (Gilley et al. 2006; Viola et al. 2011, 2012), a model of simulated steady-state recording (Mina et al. 2017), and auditory steady-state responses measured from the contralateral side of the CI device (Deprez et al. 2014, 2017b). In line with the bulk of literature documenting the efficiency of ICA in removing the CI-induced artifacts, we applied this algorithm to the recorded signals and manually selected the artifactual components to remove.

To identify the artifactual components, the scalp map, the component time-course, and the component activity power spectrum were investigated visually by the first author. Then, the artifactual components were marked based on the accepted criteria for the eye-related and CI-related component features. For the eye-related artifactual components, which predominantly can be observed as having leading positions in the IC array, the criteria included having far-frontal projections on the scalp map and a decreasing EEG spectrum observed in the activity power spectrum. The most challenging part was related to identifying the CI-related artifacts. For this step, the criteria were mostly observing continuous oscillatory activities with a narrow scalp distribution around the CI device. Figure 2 depicts some samples of CI-related artifactual components observed among our participants. Note the continuous oscillatory activities around 20 to 30 Hz in the activity power spectrum of each sample, which are more likely related to the power-up supply of the CI device. To have the agreement of all the authors on the component selection procedure and to have a reference for the later analysis, screenshots of all the suspicious artifactual components for each participant were taken and stored in an excel sheet. After having the agreement of the last author on the selected components, the artifactual components were removed, and the event-related data for each participant was examined as a confirmatory step of artifact removal. On average, 4 ($\pm$1.9) ICA components were removed from the CI group datasets. Note that the ICA algorithm was performed once, but the total number of discarded components in CI users (both eye- and CI-related components) was more than controls (with only eye-related discarded components).

SS-EPs Analysis

Channels that were initially removed in the step before the ICA were interpolated from the surrounding channels via spherical interpolation. Then, the preprocessed data was exported to Letswave 6 (www.letswave.org) running under MATLAB 2017b (The MathWorks, Natick, MA, USA) for further analysis. An FFT multi-Notch filter centered on 60 Hz, with its 10 harmonics and with a width of 1 Hz, was used to remove the electric line noise artifact. The filtered EEG epochs for each participant were averaged in the time domain across trials. This averaging was done to increase the signal to noise ratio of the recorded EEG responses and reduce signals that were not phase-locked to the auditory stimulus train (Mouraux & Iannetti 2008). To estimate SS-EP amplitudes, frequency domain analysis was performed on the obtained average using discrete Fourier transform, (DFT) followed by a baseline correction procedure (Nozaradan et al. 2011). This method was used to remove the contribution of noise by subtracting the averaged amplitude of the surrounding non-adjacent frequency bins, ranging from $\pm$3 to $\pm$5 frequency bins relative to each frequency bin across the x-axis of the spectra. The rationale behind this approach stems from the fact that, in the absence of SS-EPs, the amplitude at a given frequency bin and the averaged amplitude of the surrounding frequency bins should be similar. Therefore, lack of response to the input stimulus might result in a zero-amplitude signal for the noise-subtracted frequency bins (Mouraux et al. 2011).

To assess the magnitude of the SS-EPs and maximize the signal to noise ratio, we first averaged the signal over three different EEG channels (Fz, FCz, Cz). These three channels were selected as previous studies confirmed that a) electrodes positioned at midline frontal areas capture most of SS-EPs (Skoe & Kraus 2010b), and b) they are located far enough from the CI device. In the next step, we extracted the maximum amplitude values measured in a range of three bins centered on the target frequencies from the noise-subtracted spectrum for each participant (i.e., 2.35 – 2.45 Hz targeting 2.4 Hz and 164.95 – 165.05 Hz targeting 165 Hz). These ranges have been selected because of possible spectral leakage during signal amplitude estimation by DFT. Spectral leakage might happen as a result of frequency shift between the frequency of the fast Fourier transform (FFT) filter and its corresponding signal component or due to small fluctuations of the response over the cycles throughout the stimulus sequences (George & Bones, 1991). It could also happen if the time window on which the FFT is computed does not contain an integer number of cycles of the target frequency,

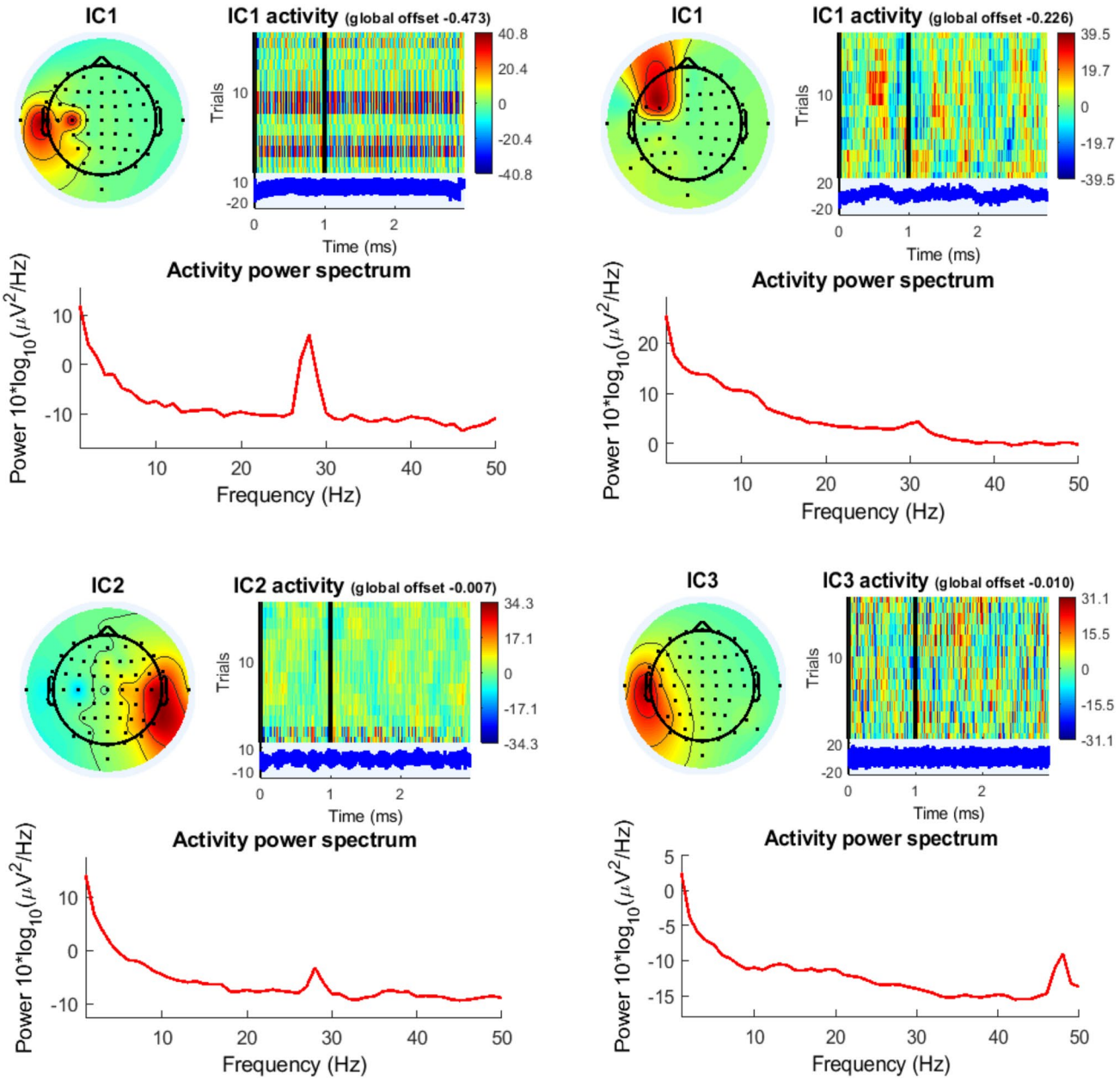

Fig. 2 Four examples of the output of Infomax algorithm showing the CI-related artifactual components across different CI users. Each example displays information about the scalp topography, the time-course of the component, and the component activity power spectrum. Note the continuous oscillatory activity around 20 to 30 Hz on the component activity power spectrum of each subplot, which are more likely related to the power-up supply of the CI device

which is not the case in the current experiment as our stimulus contains exactly 72 periods of the 2.4 Hz frequency. We used the same approach as in the previous works (Nozaradan et al. 2016a, b) to determine the number of significant harmonics in the neural response. Based on visual inspection, we extracted all observable harmonics in the group-level averaged FFT. This resulted in defining target frequencies as the harmonics of 165 Hz up to the 6th harmonics and the harmonics of 2.4 Hz up to the 10th harmonics. Then, in order to maintain the same number of harmonics across groups, we determined the highest significant harmonic elicited in the control group. The control group was selected as the reference group in order to ensure that the selected harmonics were of true neural origin and not attributable to CI-induced artifacts. To do so, all target harmonics amplitudes were tested against zero using t-tests. Only harmonics significantly above 0 μV in the noise-subtracted EEG spectra from the control group were considered for further

comparisons. As a result of this procedure, amplitude values extracted at 2.4 Hz up to the 5th harmonics and 165 Hz up to the 5th harmonics were selected for further statistical comparisons.

Time Course of Cortical and Subcortical SS-EPs

To investigate the shape of the cortical and subcortical SS-EPs and to examine whether the evoked responses in the CI group had similar waveform morphology to the responses recorded from the controls (i.e., whether SS-EPs originated from neural sources), the time course of the recorded responses of all participants at Fz, FCz, Cz channels were analyzed. The preprocessed EEG signals of the three selected electrodes were filtered using band-pass IIR Butterworth zero-phase filters (24 dB/octave, 4th order) at 0.3–30 Hz and 156–670 to obtain the time course of the cortical and subcortical responses to the sound envelope respectively. After extracting the envelopes of responses, epochs of both sets of cortical and subcortical SS-EPs were segmented into chunks of 416 ms long (duration of one sound event in the sound sequence). Within each epoch, segmentation started at + 832 ms relative to the onset of the sound yielding 1,120 time chunks for each individual dataset. This time window was selected to discard the evoked potentials induced by the onset of the sound stimulus and thus start the analysis on the response to the third sound of the sequences. Finally, the three-channels averaged waveform was calculated and used for between-group comparisons.

Statistical Evaluation

Statistical analyses were performed using SPSS statistics (IBM Corp V. 23.0; Armonk, NY). For descriptive measures, data are expressed as the mean ± standard deviation (SD). Statistical analyses were performed step-by-step with respect to the objectives of the study. First, one-sample t-tests were performed on the amplitude values of both sets of frequencies and their harmonics. This analysis was performed in an attempt to evaluate the presence of significant SS-EP responses at target frequencies. As a conservative approach, p-values below 0.005 were considered significant. In the next step, and to compare the results of time-domain analyses, cluster-based permutation tests were performed on the waveforms of both groups (using point-by-point between-subject ANOVA F-statistics). This step was carried out using Letswave 7 (www.letswave.org). Clusters of adjacent time points above the critical F values were identified and estimates of the selected clusters were obtained by computing the sum of the F-values constituting each cluster. Random permutation testing (1,000 times) of the participant-specific waveforms of various chunks was used to obtain a reference distribution of the cluster magnitude. This step was performed independently for each participant and used to define the cluster thresholds. In the end, the quantity of random partitions that lead to a larger cluster-level statistic than the observed p-value was obtained. If the clusters in the observed data had a magnitude exceeding the threshold of 97.5^{th} and 2.5^{th} percentiles when the t-test was used, they were regarded as significant (Maris & Oostenveld 2007; van den Broeke et al. 2015). In the next step, and to compare the measured SS-EP amplitude values across both groups of the study, one-way multivariate analyses of variance (MANOVA) tests were performed, and Bonferroni step-down (Holm) correction was applied as an adjustment for multiple comparisons. Finally, and only for the CI group, Pearson correlation analysis was performed to examine the relationship between the amplitude of cortical SS-EPs and the speech recognition scores.

Results

Significant SS-EPs Were Elicited in CI Users and Their Matched Controls

To confirm the feasibility of recording auditory SS-EPs elicited by acoustic stimuli in CI users and to evaluate whether significant SS-EP responses were elicited at target frequencies, one-sample t-tests were performed on the amplitude values of both sets of frequencies and their harmonics. As an attempt to correct for multiple comparisons, only p-values below 0.005 were considered significant. Because a lack of neural response to the input stimulus might result in a zero-amplitude noise-subtracted signal, we conducted this step separately for both groups to ensure that the average amplitudes of subcortical and cortical SS-EPs at selected frequencies (and their harmonics) would be significantly different from zero. Significance was confirmed for all target frequencies (2.4 and 165 Hz) as well as their respective harmonics up to the 5^{th} (see Table 2).

Subcortical SS-EPs Remained Contaminated by Non-Neural Artifacts

Figure 3 depicts the group-level average of the frequency spectra and topographic map of subcortical SS-EPs in both groups. As can be seen, there are clear peaks at 165 Hz in the frequency spectra of both groups, but the spectral peaks at the harmonics of the 165 Hz frequency suggest that the subcortical SS-EP activity in the CI group is compatible with CI-related artifact generators rather than neural response as observed in the matched controls (Fig. 3B). In other words, the spectra of subcortical SS-EPs in the CI group are not compatible with the neural source's characteristics as they do not reflect the expected pattern of neural

Table 2 T-test against zero of the average amplitudes of subcortical and cortical SS-EPs across both groups of the study

Amplitude	CIs	Controls
Subcortical SS-EPs at 165 Hz	t = 2.6, p = 0.020 [ns]	t = 7.1, p = 0.000
Subcortical SS-EPs at 330 Hz	t = 3.1, p = 0.009 [ns]	t = 5.4, p = 0.000
Subcortical SS-EPs at 495 Hz	t = 2.5, p = 0.024 [ns]	t = 4.3, p = 0.001
Subcortical SS-EPs at 660 Hz	t = 5.1, p = 0.000	t = 3.5, p = 0.004
Subcortical SS-EPs at 825 Hz	t = 1.5, p = 0.152 [ns]	t = 3.7, p = 0.003
Subcortical SS-EPs at 990 Hz	t = 1.7, p = 0.119 [ns]	t = 2.4, p = 0.029 [ns]
Cortical SS-EPs at 2.4 Hz	t = 7.6, p = 0.000	t = 6.2, p = 0.000
Cortical SS-EPs at 4.8 Hz	t = 5.0, p = 0.000	t = 4.7, p = 0.000
Cortical SS-EPs at 7.2 Hz	t = 4.1, p = 0.001	t = 5.6, p = 0.000
Cortical SS-EPs at 9.6 Hz	t = 8.9, p = 0.000	t = 5.4, p = 0.000
Cortical SS-EPs at 12 Hz	t = 4.8, p = 0.000	t = 4.4, p = 0.001
Cortical SS-EPs at 14.4 Hz	t = 4.6, p = 0.000	t = 3.2, p = 0.006 [ns]

SS-EPs steady-state evoked potentials

$p < 0.005$ was considered as significant

low-pass attenuation of harmonics (i.e., lower amplitudes at higher harmonics). This confirms the inability of the ICA algorithm to isolate true neural SS-EP peaks at 165 Hz and beyond from the CI-induced artifacts.

Likewise, the observed pattern in the group-level topographic map of CIs (Fig. 3A) confirmed the typical pattern of left and/or right implant topography (Gilley et al., 2006; Deprez et al. 2014, 2017a; Gransier et al. 2016), implying that despite our best efforts in ICA-based removal, CI-related artifacts clearly subsided in the observed response at 165 Hz. By examining the individual topographic map of subcortical SS-EPs, we found considerable variability across CI participants for the waveform morphology and scalp distribution of components at 165 Hz, but, in all participants, the artifacts were centered near the implant side. Therefore, despite the clear subcortical SS-EPs in the control group, we were not able to quantify the difference between the amplitudes of subcortical SS-EPs in two groups. This step was thus discarded due to the presence of CI-induced artifacts in the subcortical SS-EPs of our CI group.

Cortical SS-EPs of Neural Origin Were Successfully Recorded in CI Users, as Assessed by Spectra, Topographic Maps, Time-Domain Analysis

Figure 4 illustrates the group-level average of the frequency spectra and topographic map of the cortical SS-EPs in both groups. As can be seen, we found clear peaks in the spectral amplitude at 2.4 Hz and its harmonics in response to the auditory input in both groups (Fig. 4B). In addition, the observed pattern in the group-level topographic map of the harmonic frequencies in CIs was similar to the control group (Fig. 4A).

To verify whether the measured cortical SS-EPs had a neural origin in the CI group, the time courses of cortical responses were computed and compared across both groups. Figure 5A illustrates the group-level average of the event-related potential (ERP) waveforms relevant to each rhythmic period in CIs and their controls. Both CIs and control group had clear time-domain evoked-responses with qualitatively similar and observable peaks and troughs over the 416 ms time window, confirming the neural origin of cortical response in CI users.

To investigate the possible differences between the ERP waveforms of each sound onset, a series of between-subject ANOVA cluster-based permutation tests were performed on cortical responses. This method allowed us to conduct a point-by-point comparison between the cortical responses taken from both groups (Maris & Oostenveld 2007; van den Broeke et al. 2015). The technique assumes that neural activity leads to signal changes over adjacent time points and, therefore, the envelope of signals might reflect these signal changes over time (Groppe et al. 2011). ANOVA between-groups permutation test revealed that the cortical responses were significantly different in the temporal window spanning 54 to 220 ms ($p = 0.01$) and 254 to 416 ms ($p = 0.01$) between two groups.

Upon request of an anonymous reviewer, a complementary analysis was conducted to investigate the cortical mechanisms involved in auditory temporal processing, by estimating the cortical sources related to SS-EPs (Debener et al. 2008; Farahani et al. 2019, 2020). To perform the source localization analysis, the preprocessed EEG signals of all electrodes were filtered using band-pass IIR Butterworth zero-phase filters (24 dB/octave, 4th order) at 0.3–30 Hz. Then the envelope of the responses was extracted, and the epochs of cortical SS-EPs were segmented into chunks of 416 ms long. Similar to the time-course analysis, segmentation within each epoch started at + 832 ms relative to the onset of the sound yielding 1120 time chunks for each individual dataset. In the next step, all the time chunks were averaged in each individual dataset. Finally, the averaged waveform of all participants was calculated and used for the source localization analysis. The data was imported into the Brainstorm software (Tadel et al. 2011) and the cortical head models specific for each group were reconstructed for brain mapping. The head model was created based on the ICBM152 template anatomy and the default channel location file (Biosemi 64 channels, 10–10 international system) implemented in the Brainstorm software (Evans et al. 2012; Tadel et al. 2019).

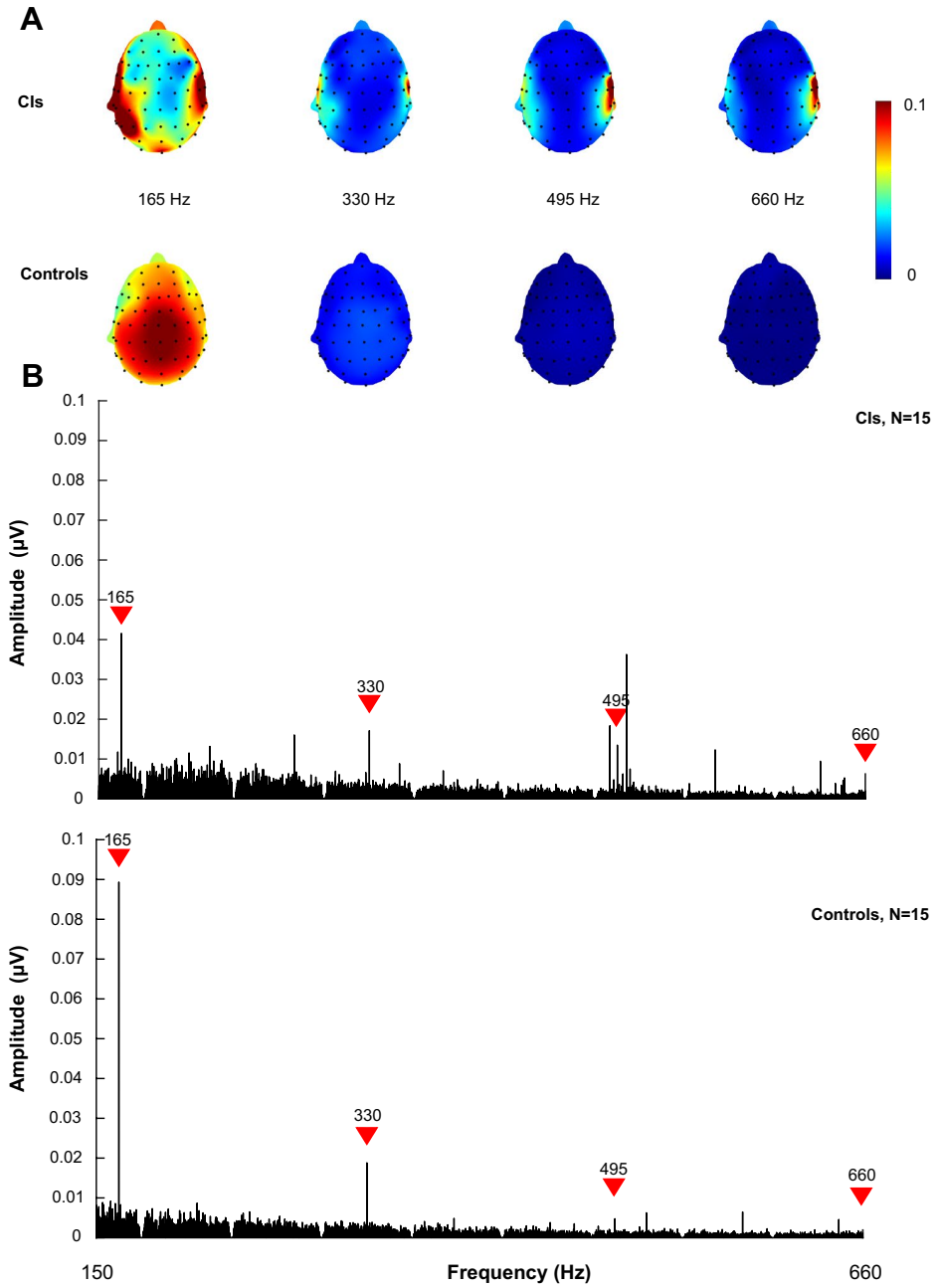

Fig. 3 **A** Excerpt of the scalp topography of subcortical SS-EPs of CIs (top row) and controls (bottom row) at 165 Hz and its harmonics (4 harmonics are shown here). **B** The frequency spectra of CIs (top panel) and controls (bottom panel) within 150 – 660 Hz showing peaks at 165 Hz along with its harmonics. SS-EPs: steady state evoked potentials, CI: cochlear implant

In the next step, the noise covariance was estimated based on no noise modeling, and the data covariance was computed from recording. The cortical head model involved three compartments, including brain, skull, and scalp, and was created by recruiting the OpenMEEG and the boundary element method (Gramfort et al. 2010). The conductivity values were defined as 0.33, 0.0041, and 0.33 S/m for the three compartments, respectively. It is believed that the greatest portion of the neural activity in the EEG-recorded signal comes from the pyramidal neurons; therefore, the surface model for the cortex was created based on a dipole orthogonal to the surface. Then, the brain source activities were reconstructed by recruiting dynamic statistical parametric mapping (dSPM) (Dale et al. 2000) implemented in the Brainstorm software. For calculating the matrix of reconstructed sources, the imaging kernel obtained from the Brainstorm software multiplying by the data of the 64-channel data. The regularization parameter required for the dSPM source estimation was set at 3.00 for the signal-to-noise ratio. Figure 5.B and C represent the reconstructed cortical sources of SS-EPs of two groups of the study at both hemispheres. As shown in the brain maps,

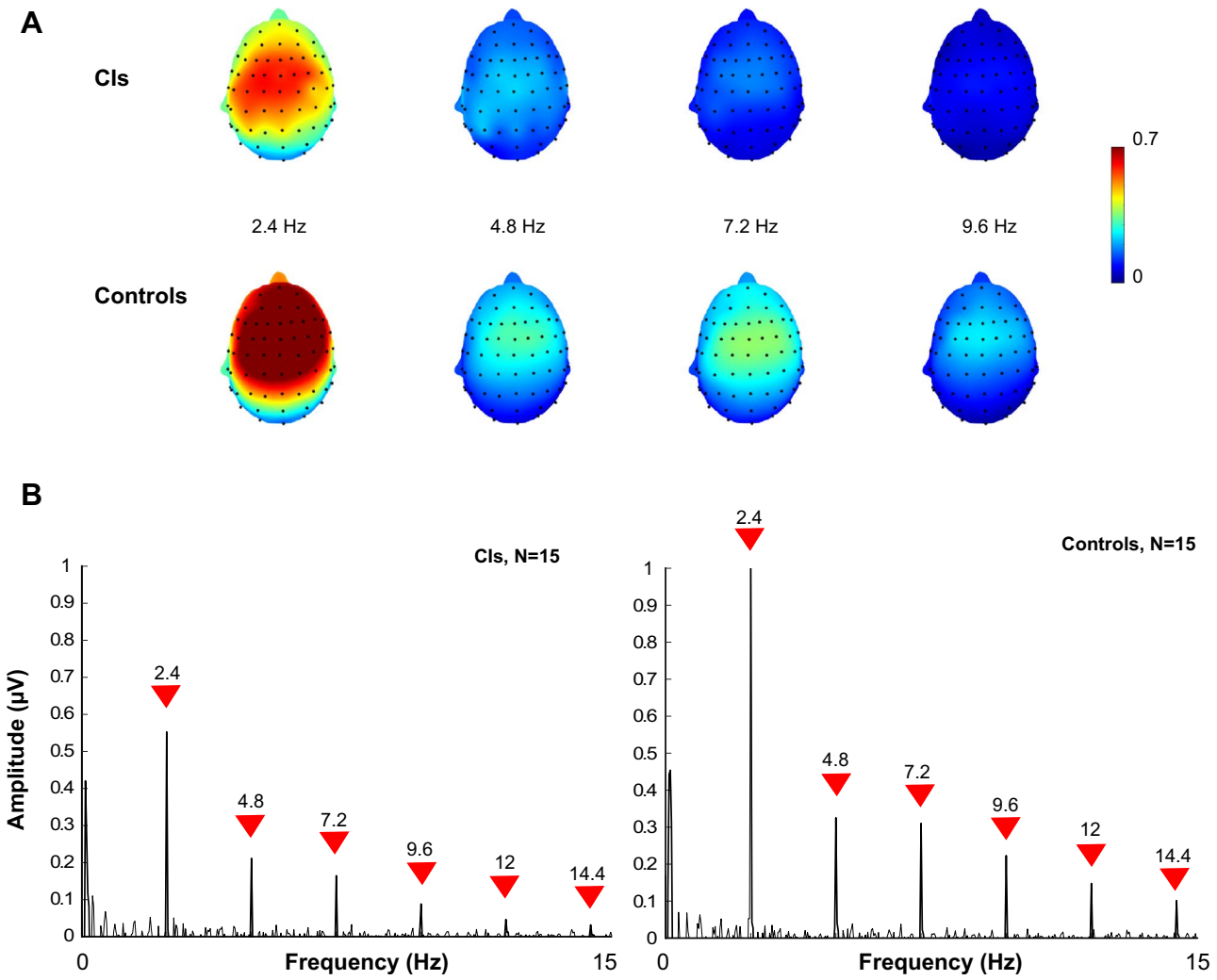

Fig. 4 **A** Excerpt of scalp topography of cortical SS-EPs of CIs (top row) and controls (bottom row) at 2.4 Hz and its harmonics (4 harmonics are shown here). **B** The frequency spectra of CIs (left panel) and controls (right panel) within 0 – 15 Hz showing peaks at 2.4 Hz along with its harmonics. SS-EPs: steady state evoked potentials, CI: cochlear implant

the pattern and locations of cortical activations in the CI users is similar to the control group, albeit with more focused activations in the controls.

After assessing the neural origin of cortical SS-EPs, a MANOVA test was conducted to examine whether the two groups were different in the amplitude of cortical SS-EPs. Prior to conducting the MANOVA, a series of Pearson correlations were performed between all values in order to test the MANOVA assumptions. The meaningful pattern of correlations observed among most of the amplitude values confirmed the appropriateness of a MANOVA. The observations resulting from this analysis corroborated the results obtained from the time domain analysis ($F(5, 24) = 2.7$, $p = 0.044$, $\eta 2 = 0.361$), indicating significant differences in the amplitude of the neural responses across groups. To gain insight into the details of the differences between the harmonic content of the evoked activity across the two groups, a series of one-way ANOVAS was conducted as a follow-up test to the MANOVA on each of the five harmonic values. The cortical SS-EP amplitudes were significantly lower in CIs (about 50 percent smaller) compared to controls at 2.4 Hz ($CIs = 0.55 \pm 0.3$, $controls = 1.06 \pm 0.7$, corrected $p = 0.04$). Moreover, the two groups significantly differed in amplitude at the 4th and 5th harmonics (corrected $p = 0.04$, corrected $p = 0.03$, respectively, in favor of the control group). No significant differences were found for the 2nd and 3rd harmonics (corrected $p > 0.056$) (Fig. 6). In addition, Pearson correlation was performed to evaluate the relationship between the amplitude values of cortical SS-EPs at 2.4 Hz and speech

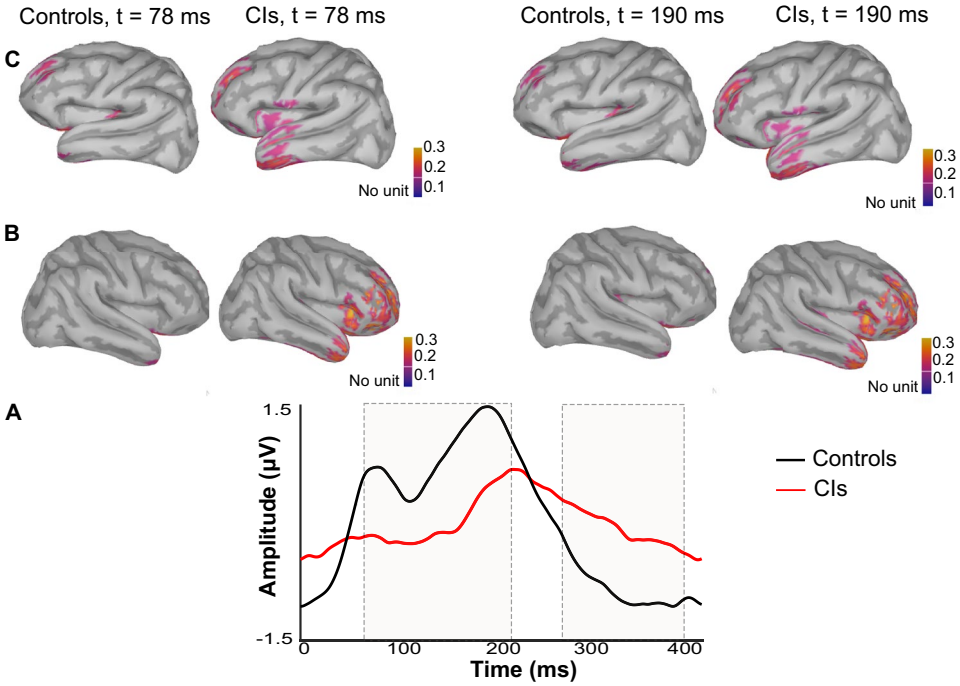

Fig. 5 The reconstructed map and time course of cortical SS-EPs (group-level average) of CIs and matched controls on the left and right hemispheres. **A** The 416-ms chunk corresponds to the window between each sound onset. The cortical responses were obtained by filtering the EEG between 0.3 and 30 Hz, an average of three midline electrodes. Gray rectangles show the temporal windows where the two groups were significantly different. **B** & **C** Reconstructed brain maps, based on 64 EEG electrodes, at both hemispheres (corresponding to the first and second peaks in A. using dSPM. SS-EPs: steady state evoked potentials, CI: cochlear implant, dSPM; dynamic statistical parametric mapping

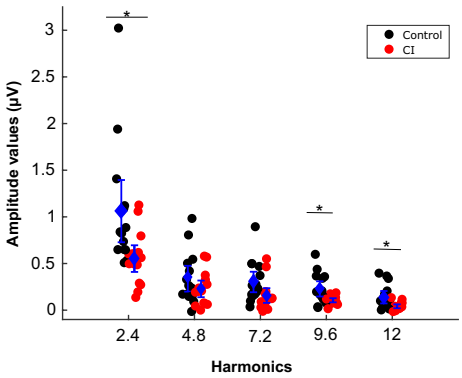

Fig. 6 Scatter plot illustrates the individual amplitude values and group's mean and SDs (blue whiskers) of cortical SS-EPs at 2.4 Hz up to 5th harmonics in CIs and matched controls. The cortical SS-EP amplitudes were significantly lower in CIs than in controls at 2.4 Hz, 9.6 Hz. And 12 Hz *: $p \leq 0.05$, SS-EPs: steady state evoked potentials, CI: cochlear implant

recognition scores of CIs. However, no significant correlation was found between them ($p > 0.05$).

Discussion

In the current study, we investigated the evoked neural responses in both subcortical and cortical sources to complex auditory amplitude-modulated tones in CI users and matched controls. Using a dual frequency-tagging approach with 165 and 2.4 Hz frequencies, we isolated subcortical and cortical SS-EPs evoked by the auditory stimuli from the scalp-recorded data, consistent with our previous results (Lehmann et al., 2016; Nozaradan et al. 2016a, b, 2018). Although we measured reliable subcortical and cortical SS-EPs in control group, the subcortical responses of some CIs were heavily contaminated by CI-induced artifacts. Consequently, only cortical SS-EPs were compared between groups, which were found to be significantly larger in the controls.

Challenges in Recording SS-EPs from CI Users

When it comes to measuring electrophysiological responses of an electrode-ear interface, limitations hinder the interpretation of the results, as the CI produces artifacts that can be difficult to separate from the biological neural responses. This is further complicated by the fact that both the artifacts and the concurrent physiologic responses in CI users are time-locked to the sound stimuli (Gilley et al. 2006). Gransier et al. (2016) recorded neural responses to pulse train stimuli modulated between 1 – 100 Hz. The authors performed two levels of analysis to remove CI stimulation artifacts from the recorded data. At first, they used a blanking method (Hofmann & Wouters 2010) to linearly interpolate the pre- and post-stimulus samples. Then, they measured phase delay across the modulation frequencies and used it as a tool to mark the residual artifacts left by the interpolation analysis step. Nevertheless, the authors reported that they were only able to measure EASSRs from the electrodes contralateral to the CI, mostly in response to

the 30 – 50 Hz range of frequency modulation. Later on, Deprez et al. (2017a) used subthreshold stimuli to discard the possibility of having neural responses and merely record CI-induced artifacts. This step was done in an attempt to characterize the device-related artifacts of EASSRs. The authors used the same linear interpolation method as in the previous study and defined three indexes for artifact classification, referred to as the amplitude growth function slope and its intercept and the duration of the artifact. Even so, the authors were only able to remove artifacts at the contralateral side of the implant and, hence, rejected the efficacy of the linear interpolation method in eliminating the artifacts at the ipsilateral side of the CI device. In both studies, the experimenters recorded EASSRs in a very controlled condition as they directly delivered the high-rate pulse trains to the CI electrode array and bypassed the device's sound coding. Nevertheless, they failed to remove the CI-stimulation artifacts from the signal recorded at the device's ipsilateral side. In contrast, in the current study, we presented the stimuli from a speaker located at the implant side and used the ICA algorithm to pinpoint and remove CI-induced artifacts. By doing so, we expected to measure the brain responses under a naturalistic condition, where the device speech processor coded the acoustical input into electrical signals.

Attina et al. (2017) evaluated the efficacy of the ICA algorithm by adding CI artifacts, recorded from a phantom equipped with CI, to ASSRs recorded from normal-hearing participants. Based on their results, the authors proposed a model to suppress electrical stimulation artifacts from the recorded ASSRs and implemented it on the data recorded from two CI users. The authors claimed that ICA was successful in detecting the CI-induced artifactual components, without affecting the characteristics of the evoked responses. However, similar to the studies mentioned earlier, the authors presented the auditory stimuli via direct streaming to only two CI users who had the same CI device brand. In a similar concept and using a computational approach, Mina et al. (2017) compared the efficacy of different ICA algorithms on the recorded ASSRs and showed that infomax ICA was highly efficient in removing CI-induced artifacts from the recorded evoked potentials.

In the current study, infomax ICA was successful when applied on the cortical potentials but failed to separate the artifactual components derived from CI stimulation from the recorded subcortical SS-EPs, as illustrated in Fig. 3, especially for subcortical SS-EPs elicited at higher frequencies. While the amplitude was expected to reduce over those higher harmonics (Wieser et al. 2016), as observed for the control group of the current study, this was not the case for the CI group, which is compatible with substantial residual artifacts produced by the CI.

The inability of the ICA algorithm to remove CI-induced artifacts from the subcortical responses might be due to the smaller amplitude of subcortical SS-EPs compared to cortical ones. As seen in Fig. 5A, the morphology of the average time course of cortical SS-EPs of CIs is similar to the one of controls confirming that ICA substantially removed artifactual components from the cortical responses in CI datasets.

The second reason could be related to the preprocessing pipeline of the current study. It has been suggested that high pass filtering between 1 – 2 Hz could increase the signal-to-noise ratio and hence, enhance the decomposition quality while performing the ICA (Winkler et al. 2015). In our preprocessing pipeline, we used a 0.1 Hz high-pass IIR Butterworth filter to remove slow drifts, and this might have affected the ICA performance.

Moreover, it seems that the challenge of isolating artifacts from brain responses might be more burdensome than initially believed when one considers the different types of CI devices (i.e., speech processing algorithms; (Li et al. 2010), the various number of active electrodes or the different sound recording conditions of the experiment (i.e., sampling frequency; (Mina et al. 2017)). For instance, Deprez et al. (2014) used 8,192 Hz as the sampling frequency to record EASSRs from a single CI user and reported the ICA denoising algorithms' efficacy for removing the CI stimulation artifact. Using a similar sampling frequency on a larger sample size in our study (one vs. fifteen), we were unable to remove electrical stimulus artifacts from the subcortical SS-EPs.

The artifactual topography of our results is in line with the vast majority of findings in the literature (Gilley et al., 2006; Martin, 2007; Castañeda-Villa & James 2010), indicating a need for more sophisticated denoising algorithms. We speculated that the application of the complex, long-lasting amplitude-modulated sound stimuli made it more difficult for the ICA algorithm to isolate and remove artifacts from the recorded signals, especially for high-frequency responses. Given that the artifacts last within the time frame of the stimulus and with an amplitude 5–10 times larger than that of the averaged response (Gilley et al. 2006), labeling artifactual components by current denoising algorithms is not entirely possible and might only be useful for suppressing artifacts at the contralateral side of the CI device. Moreover, we observed that although the topographical maps show artifacts centered near the implant side, the three selected channels taken for amplitude comparison were not far enough from the implant side to be immune from the artifacts.

The Amplitude of SS-EPs was Reduced in CI Users

Despite extensive challenges in obtaining subcortical SS-EPs in our CI users, we have successfully recorded clear cortical SS-EPs from this group in response to the 2.4 Hz

modulation frequency. We found that the amplitudes of the recorded cortical SS-EPs in CI users were significantly lower than those of their matched control.

The lower amplitude in the cortical SS-EPs of the CI group might indicate a reduction in neural synchrony evoked by the modulation rate of the auditory input across different neural assemblies in the auditory pathway of CI users (Polich 2007; Gransier et al. 2016). The auditory cortex shapes the perceptual representation of external sounds based in part on their acoustical analysis (Budinger & Kanold 2018). Evidence in support of the intricacy of the cortical neural circuity is convincing where the highly specific patterns of the inter- and intra-laminar connectivity within the auditory cortex provide precise temporal and spectral responses to the perceived stimuli (Barbour & Callaway 2008). Indeed, temporal modulation processing depends on the columnar and laminar transformation of the input information across cortical layers (Atencio et al. 2009; Atencio & Schreiner 2010). The well-organized six-layered auditory cortex possesses neuronal architectures with priorities to process specific input parameters (Wu et al. 2011), in which layers IIIb/IV, the granular layers, are the primary hubs to receive thalamic information. These hubs subsequently communicate with other neurons in the supragranular and infragranular layers and shape structural and functional corticocortical and corticothalamic connections (Budinger & Kanold 2018). Accordingly, the loss of sensory input might lead to a very basic inter-intralaminar connectivity within neural assemblies of the auditory cortex or impose substantial challenges in the case of lost sensory input (Petrus et al. 2015). Therefore, the lower cortical SS-EPs amplitude in CIs might reflect less affluent connectivity within cortical layers and the following feedforward and feedback loops.

On the flip side, sensory systems have shown significant potential to adapt to new environments (Henschke et al. 2018), such as the auditory cortex's ability to accurately decipher the information transferred by the electrical stimulation of the auditory nerve provided by the CI. Furthermore, it has been shown that CI and subsequent hearing experience increase neural synchrony while decreasing neural conduction time (Martin et al. 2008; Sandmann et al. 2015). Nevertheless, it appears that the experience-related changes after sensory stimulation in adult CI users reach a plateau after one year of implant use (Hamzavi et al. 2003; Wooi Teoh et al. 2004). Therefore, the lower SS-EP amplitudes in the CI group might also reflect a CI-user-specific ceiling effect.

Another reason for this lower amplitude could be due to a fundamental difference in the auditory spatial receptive field of the two groups of the study. Most CI users had a unilateral CI device, whereas control participants received the auditory stimuli from both ears. Accordingly, SS-EPs from both hemispheres were summated at the midline electrodes for the control group because of the orientation of the source activations in each temporal lobe (Skoe & Kraus, 2010b). But in CI users, there is a possibility that SS-EPs dominated on the contralateral hemisphere, as the ipsilateral response is smaller in unilateral stimulation. Therefore, the smaller SS-EP amplitude in CI users could be resulted from a weaker summation at midline electrodes.

Finally, the artifact removal procedure used in the current study might reduce the amplitude of the measured responses in CI users as the number of removed ICA components in CIs was higher than controls, and may have included a portion of neural response.

Conclusion

In the current study, we examined the response of auditory subcortical and cortical neurons to periodic amplitude-modulated sounds in adult CI users and their matched controls. The findings of the current study highlight the need for a different technique to record acoustically evoked subcortical potentials in CI users, rather than presenting stimuli via direct streaming. Presenting stimuli through a cable-free connection could increase the simplicity of the testing protocol and subsequently enhance the quality of the responses by decreasing the fatigue caused by a long testing period (Gama et al. 2017).

By taking advantages of a novel version of the frequency-tagging approach, we measured simultaneous subcortical and cortical SS-EPs using distinct modulation frequencies presented concomitantly. Our results confirmed the reliability of this approach for differentiating between the subcortical and cortical responses in the normal-hearing listeners and constitutes one of the first demonstrations of this approach in CI users.

However, although the cortically evoked SS-EP signals were found to be reliable, we were not able to successfully disentangle CI-induced artifacts from the subcortical SS-EPs in our CI group. Nonetheless, we showed that cortical SS-EPs were reliably obtained with a similar topography and a significant amplitude reduction in CI user compared to matched controls. Our results highlight the need for more sophisticated denoising algorithms to pinpoint the artifactual components and remove them from the biological response.

We showed that although the ICA algorithm might be a competent tool for separating a signal recorded from a normal-hearing participant into its additive subcomponents, this algorithm could not be the first choice for removing CI-induced artifacts from SS-EPs, especially when dealing with low-amplitude subcortical SS-EPs. This failure of ICA in separating artifactual components from neural responses might lead to inaccurate neural response measurement or neural signal loss (Waechter et al. 2019).

Taken all together, the lack of consistency relevant to the SS-EP parameters and denoising algorithms applicable

to CI datasets across different studies clearly prevented us from drawing a firm conclusion on the efficacy of ICA as a denoising algorithm or the superiority of stimuli presenting mode to CI users. More studies on data taken from CI users are needed to assess the efficacy and reliability of the current denoising algorithms or to propose a new model to disentangle artifactual sources from brain signals (Stropahl et al. 2017).

Acknowledgements The authors would like to thank the reviewers along with Dr. Patrice Voss for his constructive comments on the first draft of the manuscript and Marie-Anne Prudhomme, Frédérik Desaulniers, and Mihaela Felezeu for their help in recruiting participants and recording data. Thanks to the Raymond-Dewar Institute and the MAB-MacKay Rehabilitation Center that made recruiting CI users for this study possible for us. The authors confirm that this paper has not been presented/published or cited elsewhere.

Author Contributions AL obtained the funding and contributed to developing the rationale and design of the study. AL coded the experiment and acquired the data. RA analyzed the data, drafted the manuscript and created the figures. A.L helped with data analysis and AL and SN contributed to editing the manuscript.

Funding This study was supported by an Incubator Award from the Centre for Research on Brain, Language and Music (CRBLM). AL is supported by a FRQS Career Grant. SN is supported by an ERC Starting Grant RHYTHM AND BRAINS (801872).

Data Availability To protect the privacy of participants, anonymized data will be available to investigators upon request.

Declarations

Conflict of interest The authors report no conflict of interest.

Ethical Approval The Research Ethics Board of the Centre for Research in Rehabilitation of Greater Montreal approved this study (CRIR-985-0714). All participants gave written informed consent and received compensation for their participation.

References

Adrian ED, Matthews BHC (1934) The Berger rhythm: potential changes from the occipital lobes in man. Brain 57(4):355–385

Alemi R, Lehmann A (2019) Middle latency responses to optimized chirps in adult cochlear implant users. J Am Acad Audiol 30(5):396–405

Atencio CA, Schreiner CE (2010) Laminar diversity of dynamic sound processing in cat primary auditory cortex. J Neurophysiol 103(1):192–205

Atencio CA, Sharpee TO, Schreiner CE (2009) Hierarchical computation in the canonical auditory cortical circuit. Proc Natl Acad Sci 106(51):21894–21899

Attina V, Mina F, Stahl P, Duroc Y, Veuillet E, Truy E, Thai-Van H (2017) A new method to test the efficiency of Cochlear Implant artifacts removal from Auditory Evoked Potentials. IEEE Trans Neural Syst Rehabil Eng 25(12):2453–2460

Barbour DL, Callaway EM (2008) Excitatory local connections of superficial neurons in rat auditory cortex. J Neurosci 28(44):11174–11185

Beck AA, Rossion B, Samson D (2018) An objective neural signature of rapid perspective taking. Soc Cogn Affect Neurosci 13(1):72–79

Bidelman GM (2015) Multichannel recordings of the human brainstem frequency-following response: scalp topography, source generators, and distinctions from the transient ABR. Hear Res 323:68–80

Budinger E, Kanold PO (2018) Auditory Cortex Circuits. The Mammalian Auditory Pathways. Springer, Cham, pp 199–233

Castañeda-Villa N, James CJ (2010) Independent component analysis for auditory evoked potentials and cochlear implant artifact estimation. IEEE Trans Biomed Eng 58(2):348–354

Clark G (2004) Cochlear Implants. In: Greenberg Steven, Ainsworth William A, Fay Richard R (eds) Speech Processing in the Auditory System. Springer Handbook of Auditory Research, New York, p 18

Coffey EBJ, Nicol T, White-Schwoch T, Chandrasekaran B, Krizman J, Skoe E, Kraus N (2019) Evolving perspectives on the sources of the frequency-following response. Nat Commun 10(1):1–10

Dale AM, Liu AK, Fischl BR, Buckner RL, Belliveau JW, Lewine JD, Halgren E (2000) Dynamic statistical parametric mapping: combining fMRI and MEG for high-resolution imaging of cortical activity. Neuron 26(1):55–67

Debener S, Hine J, Bleeck S, Eyles J (2008) Source localization of auditory evoked potentials after cochlear implantation. Psychophysiology 45(1):20–24

Delorme A, Makeig S (2004) EEGLAB: an open source toolbox for analysis of single-trial EEG dynamics including independent component analysis. J Neurosci Methods 134(1):9–21

Deprez, H., Hofmann, M., Van Wieringen, A., Wouters, J., & Moonen, M. (2014). Cochlear implant artifact rejection in electrically evoked auditory steady state responses. In 2014 22nd European Signal Processing Conference (EUSIPCO) (pp. 1995–1999). IEEE.

Deprez H, Gransier R, Hofmann M, van Wieringen A, Wouters J, Moonen M (2017a) Characterization of cochlear implant artifacts in electrically evoked auditory steady-state responses. Biomed Signal Process Control 31:127–138

Deprez H, Gransier R, Hofmann M, van Wieringen A, Wouters J, Moonen M (2017b) Independent component analysis for cochlear implant artifacts attenuation from electrically evoked auditory steady-state response measurements. J Neural Eng 15(1):16006

Echtioui, A., Zouch, W., Ghorbel, M., Slima, M. Ben, Hamida, A. Ben, & Mhiri, C. (2020). Automated EEG Artifact Detection Using Independent Component Analysis. In 2020 5th International Conference on Advanced Technologies for Signal and Image Processing (ATSIP) (pp. 1–5). IEEE.

Evans AC, Janke AL, Collins DL, Baillet S (2012) Brain templates and atlases. Neuroimage 62(2):911–922

Farahani ED, Wouters J, van Wieringen A (2019) Contributions of non-primary cortical sources to auditory temporal processing. Neuroimage 191:303–314

Farahani ED, Wouters J, van Wieringen A (2020) Brain mapping of auditory steady-state responses: A broad view of cortical and subcortical sources. Hum Brain Mapp. https://doi.org/10.1002/hbm.25262

Gama N, Peretz I, Lehmann A (2017) Recording the human brainstem frequency-following-response in the free-field. J Neurosci Methods 280:47–53

George TA, Bones D (1991) Harmonic power flow determination using the fast Fourier transform. IEEE Trans Power Delivery 6(2):530–535

Gilley PM, Sharma A, Dorman M, Finley CC, Panch AS, Martin K (2006) Minimization of cochlear implant stimulus artifact in cortical auditory evoked potentials. Clin Neurophysiol 117(8):1772–1782

Glennon E, Svirsky MA, Froemke RC (2020) Auditory cortical plasticity in cochlear implant users. Curr Opin Neurobiol 60:108–114

Gramfort A, Papadopoulo T, Olivi E, Clerc M (2010) OpenMEEG: opensource software for quasistatic bioelectromagnetics. Biomed Eng Online 9(1):1–20

Gransier R, Deprez H, Hofmann M, Moonen M, van Wieringen A, Wouters J (2016) Auditory steady-state responses in cochlear implant users: Effect of modulation frequency and stimulation artifacts. Hear Res 335:149–160

Gransier R, Luke R, van Wieringen A, Wouters J (2020) Neural modulation transmission is a marker for speech perception in noise in cochlear implant users. Ear Hear 41(3):591–602

Groppe DM, Urbach TP, Kutas M (2011) Mass univariate analysis of event-related brain potentials/fields II: Simulation studies. Psychophysiology 48(12):1726–1737

Hamzavi J, Baumgartner W, Pok SM, Franz P, Gstoettner W (2003) Variables affecting speech perception in postlingually deaf adults following cochlear implantation. Acta Otolaryngol 123(4):493–498

Henry MJ, Obleser J (2012) Frequency modulation entrains slow neural oscillations and optimizes human listening behavior. Proc Natl Acad Sci 109(49):20095–20100

Henschke JU, Oelschlegel AM, Angenstein F, Ohl FW, Goldschmidt J, Kanold PO, Budinger E (2018) Early sensory experience influences the development of multisensory thalamocortical and intracortical connections of primary sensory cortices. Brain Struct Funct 223(3):1165–1190

Herdman AT, Lins O, Van Roon P, Stapells DR, Scherg M, Picton TW (2002) Intracerebral sources of human auditory steady-state responses. Brain Topogr 15(2):69–86

Hirschfelder A, Gräbel S, Olze H (2008) The impact of cochlear implantation on quality of life: the role of audiologic performance and variables. Otolaryngol Head Neck Surg 138(3):357–362

Hofmann M, Wouters J (2010) Electrically evoked auditory steady state responses in cochlear implant users. JARO 11(2):267–282. https://doi.org/10.1007/s10162-009-0201-z

Hofmann M, Wouters J (2012) Improved electrically evoked auditory steady-state response thresholds in humans. J Assoc Res Otolaryngol 13(4):573–589

Jeng F-C, Abbas PJ, Brown CJ, Miller CA, Nourski KV, Robinson BK (2007) Electrically evoked auditory steady-state responses in guinea pigs. Audiol Neurotol 12(2):101–112

Kuwada S, Batra R, Maher VL (1986) Scalp potentials of normal and hearing-impaired subjects in response to sinusoidally amplitude-modulated tones. Hear Res 21(2):179–192

Lehmann A, Arias DJ, Schönwiesner M (2016) Tracing the neural basis of auditory entrainment. Neuroscience 337:306–314

Lenc T, Keller PE, Varlet M, Nozaradan S (2020) Neural and behavioral evidence for frequency-selective context effects in rhythm processing in humans. Cereb Cortex Commun 1(1):tgaa037

Li, X., Nie, K., Karp, F., Tremblay, K. L., & Rubinstein, J. T. (2010). Characteristics of stimulus artifacts in EEG recordings induced by electrical stimulation of cochlear implants. In 2010 3rd International Conference on Biomedical Engineering and Informatics (Vol. 2, pp. 799–803). IEEE.

Liégeois-Chauvel C, Lorenzi C, Trébuchon A, Régis J, Chauvel P (2004) Temporal envelope processing in the human left and right auditory cortices. Cereb Cortex 14(7):731–740

Luke R, De Vos A, Wouters J (2017) Source analysis of auditory steady-state responses in acoustic and electric hearing. NeuroImage 147:568–576. https://doi.org/10.1016/j.neuroimage.2016.11.023

Luts H, Desloovere C, Wouters J (2006) Clinical application of dichotic multiple-stimulus auditory steady-state responses in high-risk newborns and young children. Audiol Neurotol 11(1):24–37

Makeig S, Onton J (2011) ERP features and EEG dynamics: an ICA perspective. Oxford Handbook of Event-Related Potential Components, Oxford

Makeig S, Bell AJ, Jung T-P, Sejnowski TJ (1996) Independent component analysis of electroencephalographic data. Adv Neural Inf Process Syst. https://doi.org/10.1007/978-1-4615-5351-9_17

Maris E, Oostenveld R (2007) Nonparametric statistical testing of EEG-and MEG-data. J Neurosci Methods 164(1):177–190

Martin BA (2007) Can the acoustic change complex be recorded in an individual with a cochlear implant? Separating neural responses from cochlear implant artifact. J Am Acad Audiol 18(2):126–140

Martin BA, Tremblay KL, Korczak P (2008) Speech evoked potentials: from the laboratory to the clinic. Ear Hear 29(3):285–313

Michel CM, Murray MM, Lantz G, Gonzalez S, Spinelli L, de Peralta RG (2004) EEG source imaging. Clin Neurophysiol 115(10):2195–2222

Milford CA, Birchall JP (1989) Steady-state auditory evoked potentials to amplitude-modulated tones in hearing-impaired subjects. Br J Audiol 23(2):137–142

Mina F, Attina V, Duroc Y, Veuillet E, Truy E, Thai-Van H (2017) Auditory steady state responses and cochlear implants: Modeling the artifact-response mixture in the perspective of denoising. PloS One 12(3):e0174462

Mouraux A, Iannetti GD (2008) Across-trial averaging of event-related EEG responses and beyond. Magn Reson Imaging 26(7):1041–1054

Mouraux A, Iannetti GD, Colon E, Nozaradan S, Legrain V, Plaghki L (2011) Nociceptive steady-state evoked potentials elicited by rapid periodic thermal stimulation of cutaneous nociceptors. J Neurosci 31(16):6079–6087

Müller MM, Andersen S, Trujillo NJ, Valdes-Sosa P, Malinowski P, Hillyard SA (2006) Feature-selective attention enhances color signals in early visual areas of the human brain. Proc Natl Acad Sci 103(38):14250–14254

Murray MM, Brunet D, Michel CM (2008) Topographic ERP analyses: a step-by-step tutorial review. Brain Topogr 20(4):249–264

Norcia AM, Appelbaum LG, Ales JM, Cottereau BR, Rossion B (2015) The steady-state visual evoked potential in vision research: A review. J vis 15(6):4

Nozaradan S (2014) Exploring how musical rhythm entrains brain activity with electroencephalogram frequency-tagging. Phil Trans R Soc B. https://doi.org/10.1098/rstb.2013.0393

Nozaradan S, Peretz I, Missal M, Mouraux A (2011) Tagging the neuronal entrainment to beat and meter. J Neurosci 31(28):10234–10240. https://doi.org/10.1523/JNEUROSCI.0411-11.2011

Nozaradan S, Zerouali Y, Peretz I, Mouraux A (2015) Capturing with EEG the neural entrainment and coupling underlying sensorimotor synchronization to the beat. Cereb Cortex 25(3):736–747

Nozaradan S, Schönwiesner M, Caron-Desrochers L, Lehmann A (2016) Enhanced brainstem and cortical encoding of sound during synchronized movement. NeuroImage. https://doi.org/10.1016/j.neuroimage.2016.07.015

Nozaradan S, Peretz I, Keller PE (2016) Individual differences in rhythmic cortical entrainment correlate with predictive behavior in sensorimotor synchronization. Sci Rep. https://doi.org/10.1038/srep20612

Nozaradan S, Schwartze M, Obermeier C, Kotz SA (2017) Specific contributions of basal ganglia and cerebellum to the neural tracking of rhythm. Cortex 95:156–168. https://doi.org/10.1016/j.cortex.2017.08.015

Nozaradan S, Keller PE, Rossion B, Mouraux A (2018) EEG frequency-tagging and input-output comparison in rhythm perception. Brain Topogr 31(2):153–160. https://doi.org/10.1007/s10548-017-0605-8

Petrus E, Rodriguez G, Patterson R, Connor B, Kanold PO, Lee H-K (2015) Vision loss shifts the balance of feedforward and intracortical circuits in opposite directions in mouse primary auditory and visual cortices. J Neurosci 35(23):8790–8801

Picard M (1997) Speech audiometry in French-speaking Quebec. Revue D'orthophonie Et D'audiologie 21(4):301–311

Picton TW, John SM (2004) Avoiding electromagnetic artifacts when recording auditory steady-state responses. J Am Acad Audiol 15(8):541–554

Picton TW, Hillyard SA, Krausz HI, Galambos R (1974) Human auditory evoked potentials. I: Evaluation of components. Electroencephalogr Clin Neurophysiol 36:179–190

Picton TW, John MS, Dimitrijevic A, Purcell D (2003) Human auditory steady-state responses: Respuestas auditivas de estado estable en humanos. Int J Audiol 42(4):177–219

Polich J (2007) Updating P300: an integrative theory of P3a and P3b. Clin Neurophysiol 118(10):2128–2148

Purcell DW, John SM, Schneider BA, Picton TW (2004) Human temporal auditory acuity as assessed by envelope following responses. J Acoust Soc Am 116(6):3581–3593

Rance Gary, Briggs RJS (2002) Assessment of hearing in infants with moderate to profound impairment: The Melbourne experience with auditory steady-state evoked potential testing. Ann Otol Rhinol Laryngol 111(5):22–28. https://doi.org/10.1177/00034894021110s505

Rance G, Rickards FW, Cohen LT, Burton MJ, Clark GM (1993) Steady state evoked potentials: a new tool for the accurate assessment of hearing in cochlear implant candidates. Adv Otorhinolaryngol 48:44–48

Rance G, Dowell RC, Rickards FW, Beer DE, Clark GM (1998) Steady-state evoked potential and behavioral hearing thresholds in a group of children with absent click-evoked auditory brain stem response. Ear Hear 19(1):48–61

Rees A, Green GGR, Kay RH (1986) Steady-state evoked responses to sinusoidally amplitude-modulated sounds recorded in man. Hear Res 23(2):123–133. https://doi.org/10.1016/0378-5955(86)90009-2

Regan D (1966) Some characteristics of average steady-state and transient responses evoked by modulated light. Electroencephalogr Clin Neurophysiol 20(3):238–248

Rossion B, Boremanse A (2011) Robust sensitivity to facial identity in the right human occipito-temporal cortex as revealed by steady-state visual-evoked potentials. J vis 11(2):16

Rossion B, Retter TL, Liu-Shuang J (2020) Understanding human individuation of unfamiliar faces with oddball fast periodic visual stimulation and electroencephalography. Eur J Neurosci 52(10):4283–4344

Sandmann P, Plotz K, Hauthal N, de Vos M, Schönfeld R, Debener S (2015) Rapid bilateral improvement in auditory cortex activity in postlingually deafened adults following cochlear implantation. Clin Neurophysiol 126(3):594–607

Skoe E, Kraus N (2010) Hearing it again and again: on-line subcortical plasticity in humans. PLoS One 5(10):e13645

Skoe E, Kraus N (2010a) Auditory brainstem response to complex sounds: a tutorial. Ear Hear 31(3):302

Stropahl M, Chen L-C, Debener S (2017) Cortical reorganization in postlingually deaf cochlear implant users: intra-modal and cross-modal considerations. Hear Res 343:128–137

Tadel F, Baillet S, Mosher JC, Pantazis D, Leahy RM (2011) Brainstorm: a user-friendly application for MEG/EEG analysis. Comput Intell Neurosci. https://doi.org/10.1155/2011/879716

Tadel F, Bock E, Niso G, Mosher JC, Cousineau M, Pantazis D, Baillet S (2019) MEG/EEG group analysis with brainstorm. Front Neurosci 13:76

Tal I, Large EW, Rabinovitch E, Wei Y, Schroeder CE, Poeppel D, Golumbic EZ (2017) Neural entrainment to the beat: The "missing-pulse" phenomenon. J Neurosci 37(26):6331–6341

Tamburro G, Croce P, Zappasodi F, Comani S (2021) Is Brain dynamics preserved in the EEG after automated artifact removal? A validation of the fingerprint method and the automatic removal of cardiac interference approach based on microstate analysis. Front Neurosci 14:1404

Torres-Fortuny A, Arnaiz-Marquez I, Hernández-Pérez H, Eimil-Suárez E (2018) Auditory steady-state response in cochlear implant patients. Acta Otorrinolaringol (english Edition) 69(5):268–274

van den Broeke EN, Mouraux A, Groneberg AH, Pfau DB, Treede R-D, Klein T (2015) Characterizing pinprick-evoked brain potentials before and after experimentally induced secondary hyperalgesia. J Neurophysiol 114(5):2672–2681

Van Maanen A, Stapells DR (2010) Multiple-ASSR thresholds in infants and young children with hearing loss. J Am Acad Audiol 21(8):535–545

Van Eeckhoutte M, Luke R, Wouters J, Francart T (2018) Stability of auditory steady state responses over time. Ear Hear 39(2):260–268

Viola FC, Thorne JD, Bleeck S, Eyles J, Debener S (2011) Uncovering auditory evoked potentials from cochlear implant users with independent component analysis. Psychophysiology 48(11):1470–1480

Viola FC, De Vos M, Hine J, Sandmann P, Bleeck S, Eyles J, Debener S (2012) Semi-automatic attenuation of cochlear implant artifacts for the evaluation of late auditory evoked potentials. Hear Res 284(1–2):6–15

Waechter, S. M., Simoes-Franklin, C., Smith, J., Viani, L., & Reilly, R. B. (2019). Cochlear implant artefact reduction in electroencephalography data obtained with the auditory oddball paradigm and stimuli with differing envelopes. In 2019 9th International IEEE/EMBS Conference on Neural Engineering (NER) (pp. 203–206). IEEE.

Wieser MJ, Miskovic V, Keil A (2016) Steady-state visual evoked potentials as a research tool in social affective neuroscience. Psychophysiology 53(12):1763–1775

Winkler, I., Debener, S., Müller, K.-R., & Tangermann, M. (2015). On the influence of high-pass filtering on ICA-based artifact reduction in EEG-ERP. In 2015 37th Annual International Conference of the IEEE Engineering in Medicine and Biology Society (EMBC) (pp. 4101–4105). IEEE.

Wooi Teoh S, Pisoni DB, Miyamoto RT (2004) Cochlear implantation in adults with prelingual deafness Part i Clinical Results. Laryngoscope 114(9):1536–1540

Wu GK, Tao HW, Zhang LI (2011) From elementary synaptic circuits to information processing in primary auditory cortex. Neurosci Biobehav Rev 35(10):2094–2104

Yao D (2001) A method to standardize a reference of scalp EEG recordings to a point at infinity. Physiol Meas 22(4):693

Zhigalov A, Herring JD, Herpers J, Bergmann TO, Jensen O (2019) Probing cortical excitability using rapid frequency tagging. Neuroimage 195:59–66

Zoefel B, ten Oever S, Sack AT (2018) The involvement of endogenous neural oscillations in the processing of rhythmic input: More than a regular repetition of evoked neural responses. Front Neurosci. https://doi.org/10.3389/fnins.2018.00095